Supporting Information for

Fusion of photodynamic therapy and photoactivated chemotherapy: a novel Ru(II) arene complex with dual activities of photobinding and photocleavage toward DNA

Yongjie Chen[a, b], Wanhua Lei[a], Guoyu Jiang[a], Yuanjun Hou[a], Chao Li[a], Baowen Zhang[a], Qianxiong Zhou*[a], Xuesong Wang*[a]

[a] Key Laboratory of Photochemical Conversion and Optoelectronic Materials, Technical Institute of Physics and Chemistry, Chinese Academy of Sciences, Beijing 100190, P. R. China

[b]Graduate School of Chinese Academy of Sciences, Beijing 100049, P. R. China

Spectroscopic Measurements

^{1}H NMR spectra were recorded on a Bruker DMX-400 MHz spectrophotometer, using $SiMe_4$ as standard. High resolution mass spectra were obtained on a Bruker APEX IV FT_MS. Elemental analysis was performed on an Elementar Vario EL instrument. UV-vis spectra were recorded on a Shimadzu UV-1601PC spectrophotometer. Fluorescence emission spectra were recorded on a Hitachi F-4500 fluorescence spectrophotometer. X-ray diffraction data were collected at 153(2) K on a Bruker Smart 1000 CCD diffractometer with Mo Kα radiation (λ = 0.71073 Å).

EPR spectra were obtained on a Bruker ESP-300E spectrometer at 9.75 GHz, X-band with 100 Hz field modulation, using TEMP as spin trapping agent. Samples were injected quantitatively into home-made quartz capillaries, then illuminated in the cavity of the EPR spectrometer with a Nd:YAG laser at 532 nm (5-6 ns of pulse width, 10 Hz of repetition frequency, 30 mJ/pulse energy).

The electrochemical properties were measured on an EG&G Model283 Potentiostat/Galvanostat in a three-electrode cell with a glassy carbon working electrode, a Pt gauze counter electrode, and a saturated calomel electrode (SCE) as reference. The cyclic voltammetry was conducted at a scan rate of 100 mV s^{-1} in N_2-saturated, anhydrous CH_3CN containing 0.1 M tetra-*n*-butylammonium hexafluorophosphate as the supporting electrolyte.

$^1O_2$ Measurement

The reaction of $^1O_2$ with DPBF was adopted to assess the $^1O_2$ generation ability. A series of 2 mL of air-saturated solutions of DPBF and the complex, of which the absorbance at 400 nm was adjusted to the same, were illuminated with the light of 400 or 550 nm (obtained from a Hitachi F-4500 fluorescence spectrophotometer). The consumption of DPBF was monitored by either absorption bleaching at 405 nm or fluorescence quenching.

DNA Electrophoresis

Supercoiled pUC19 plasmid DNA was used as target for studying DNA damage abilities of the examined complexes. 50 μL of supercoiled pUC19 DNA (40 μg/mL) was incubated with compound dosed from 0 to 100 μM. The mixture was irradiated with visible light for 30-90 minutes by a 1000 W solar simulator (Oriel 91192), using a 400 or 550 nm-long pass glass filter and a distilled water pool to cut off the UV and IR light. After irradiation, 20 μL Loading buffer was added. 10 μL of sample was taken for agarose gel electrophoresis (in Tris-acetic acid-EDTA buffer, pH 8.0) at 80 V for 1.5 h. The gel was stained with EB (1 mg/L in H_2O) for 0.5 h and then analyzed using a Gel Doc XR system (Bio-Rad).

Cellular Imaging

All tissue culture media and reagent were purchased from Hy-Clone, Thermo Scientific. The human lung carcinoma cells A549 were grown in DMEM containing 10% fetal bovine serum. Cultures were maintained at 37 ℃ under an appropriate atmosphere with 5% CO_2.

A549 cells were plated on Culture Dishes containing a microscope slide for confocal laser scanning microscopy (CLSM) observations. The cells were incubated concurrently with 5 μM of Hoechst 34580 and 5 μM of **3** for 4 h before pre-illumination (λ > 400 nm for 30 min). Then the slides were washed three times with 5 mM PBS (pH = 7.4). Fluorescence microscopy was performed on a Nikon C1Si inverted fluorescent microscope and the magnification employed was 10 × 60.

MTT Assay

A549 cells were plated at 2 *10^5 per well in a Nunc 96 well plate and allowed to grow for 24 h. The cells were exposed to increasing concentrations of complexes and incubated for 4 h, and then irradiated for 1 h at λ > 400 nm using solar simulator (70 mW/cm^2). After another 20 h of incubation, the loading medium was removed and the cells were fed with medium containing MTT from Sigma. Dark controls were run in parallel. Cell survivals were obtained by analysis of the absorbance at 490 nm using a Thermo MK3 Multiscan microplate reader. The data were normalized to 100% viable (untreated) cells.

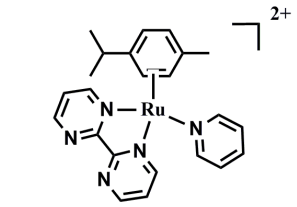

$[(\eta^6\text{-}p\text{-cymene})Ru(bpm)(py)]^{2+}$

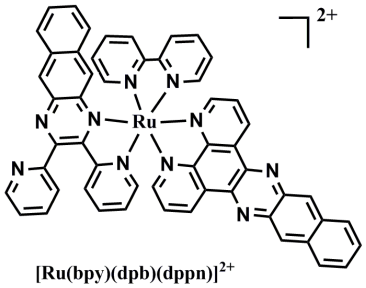

$[Ru(bpy)(dpb)(dppn)]^{2+}$

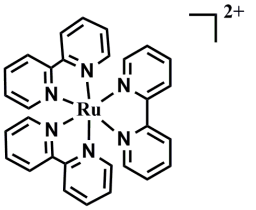

$[Ru(bpy)_3]^{2+}$

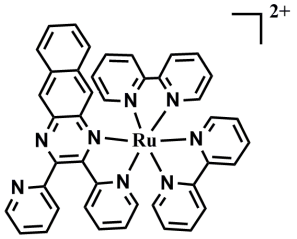

$[Ru(bpy)_2(dpb)]^{2+}$

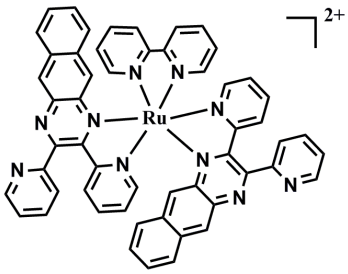

$[Ru(bpy)(dpb)_2]^{2+}$

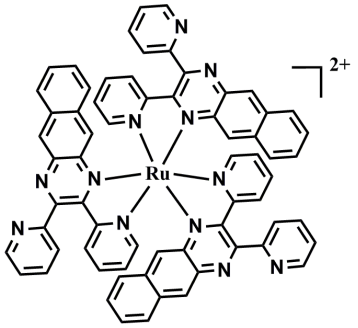

$[Ru(dpb)_3]^{2+}$

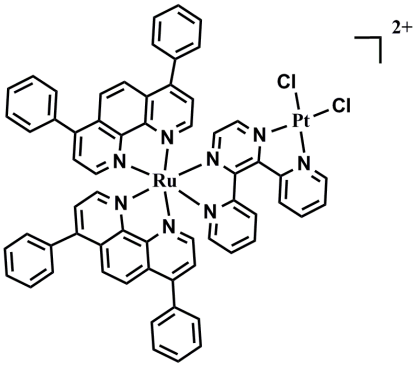

$[(Ph_2phen)_2Ru(dpp)PtCl_2]^{2+}$

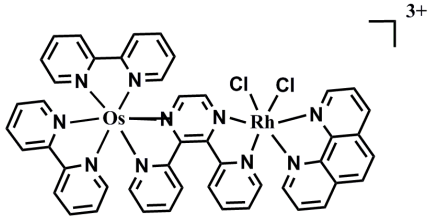

$[(bpy)_2Os(dpp)RhCl_2(phen)]^{3+}$

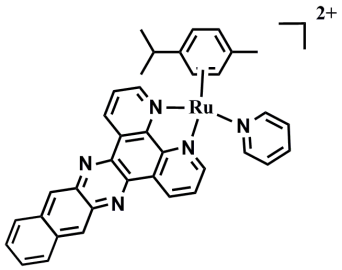

$[(\eta^6\text{-}p\text{-cymene})Ru(dppn)(py)]^{2+}$

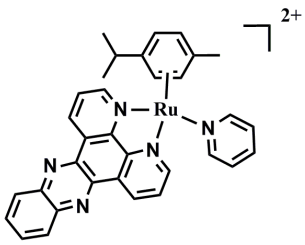

$[(\eta^6\text{-}p\text{-cymene})Ru(dppz)(py)]^{2+}$

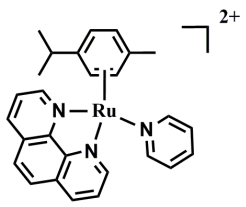

$[(\eta^6\text{-}p\text{-cymene})Ru(phen)(py)]^{2+}$

Scheme S1. Chemical structures of the complexes mentioned in this article.

Table S1. Crystal data and structure refinement parameters for **2**.

Empirical formula	$C_{33}\ H_{31}\ F_{12}N_5\ P_2\ Ru,\ 2.37(C_2\ H_3\ N)$
Formula weight	986.02
Temperature	153(2) K
Wavelength	0.71073 Å
Crystal system, space group	Orthorhombic, P2(1)2(1)2(1)
Unit cell dimensions	a = 9.941(2) Å, α = 90 deg
	b = 13.345(3) Å, β= 90 deg
	c = 31.565(7) Å, γ = 90 deg
Volume	4187.2(15) $Å^3$
Z	4
Calculated density	1.564 mg/m^3
Absorption coefficient	0.543 mm^{-1}
F(000)	1993
Crystal size	0.34 x 0.25 x 0.03 mm
θ range for data collection	2.15 to 27.00 deg
Limiting indices	$-12 \le h \le 12,\ -16 \le k \le 17,\ -40 \le l \le 39$
Reflections collected / unique	31367 / 9052 [R(int) = 0.0752]
Completeness to θ = 27.00	99.5 %
Absorption correction	Semi-empirical from equivalents
Max. and min. transmission	0.9839 and 0.8349
Refinement method	Full-matrix least-squares on F^2
Data / restraints / parameters	9052 / 0 / 567
Goodness-of-fit on F^2	1.003
Final R indices [I > 2σ(I)]	R1 = 0.0772, wR2 = 0.1910
R indices (all data)	R1 = 0.0842, wR2 = 0.1996
Absolute structure parameter	0.51(5)
Extinction coefficient	0.0057(7)
Largest diff. peak/ hole	2.676/ -1.807 e $\cdot A^{-3}$

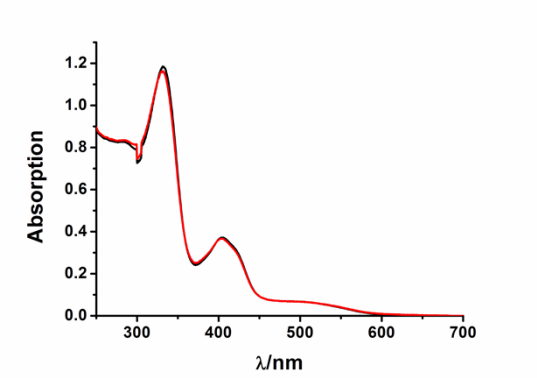

Figure S1. Absorption spectrum changes of **1** (25 μM) in PBS buffer (pH = 7.4) after standing in the dark for 4 h at room temperature.

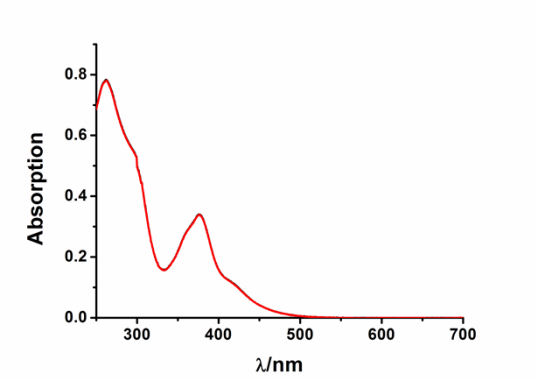

Figure S2. Absorption spectrum changes of **2** (25 μM) in PBS buffer (pH = 7.4) after standing in the dark for 4 h at room temperature.

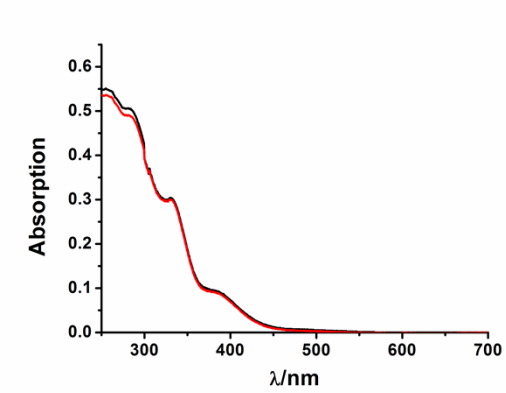

Figure S3. Absorption spectrum changes of **3** (25 μM) in PBS buffer (pH = 7.4) after standing in the dark for 4 h at room temperature.

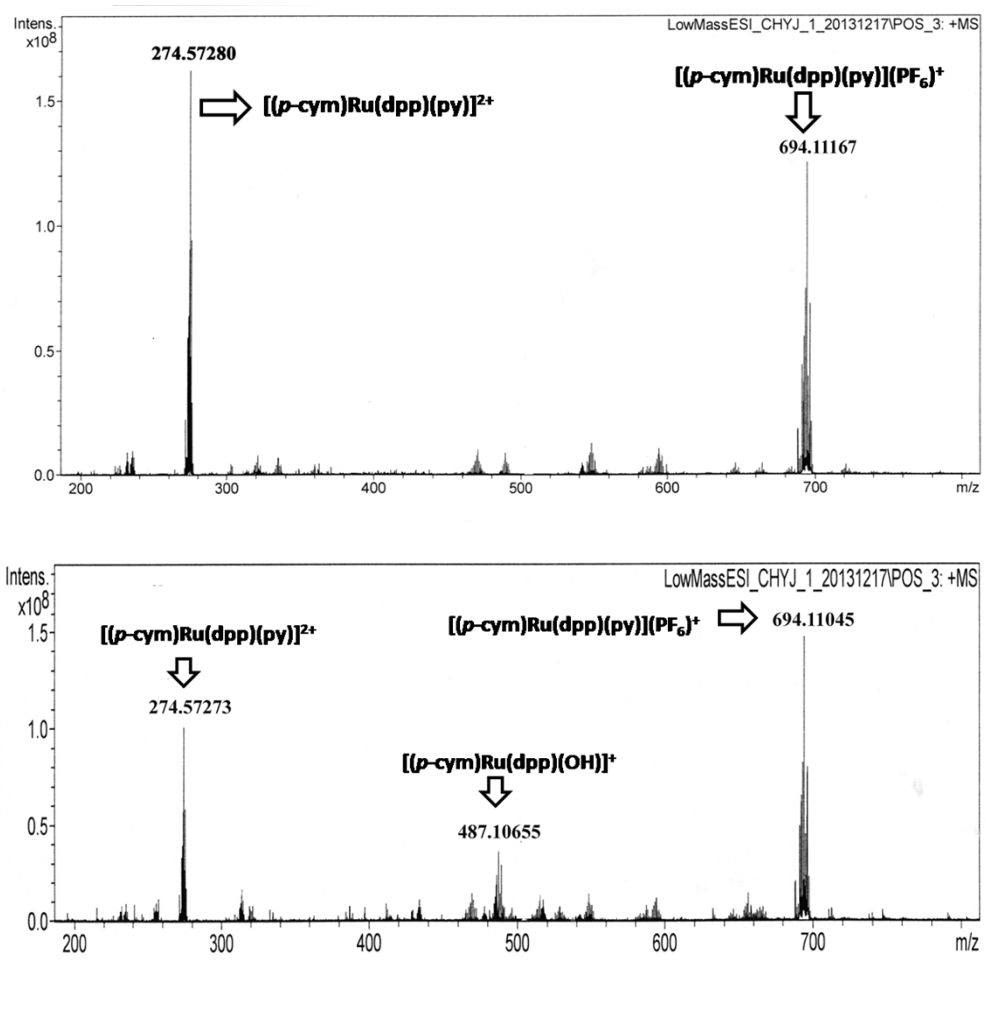

Figure S4. High-resolution ESI mass spectra of **3** in CH_3COCH_3:H_2O (1:2) before (top) and after (bottom) irradiation (λ > 400 nm) for 4 h.

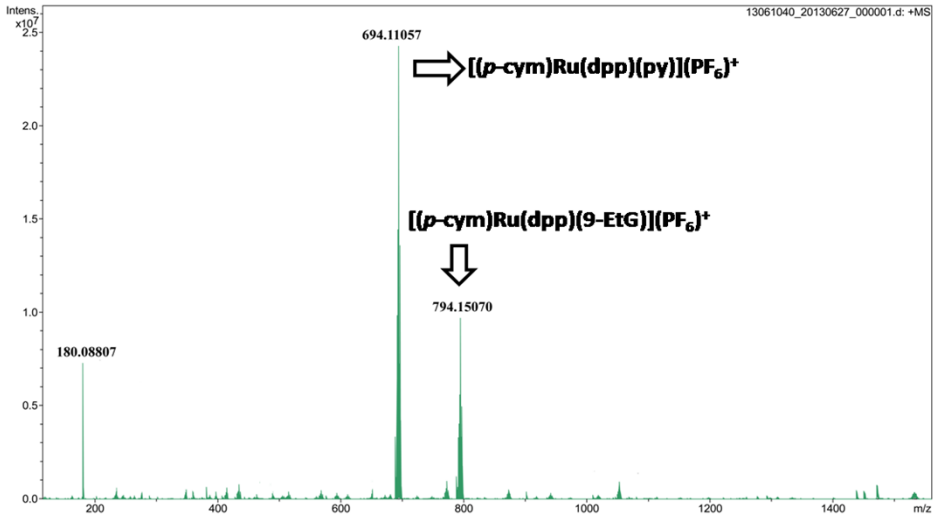

Figure S5. High-resolution ESI mass spectrum of **3** in CH_3COCH_3:H_2O (1:2) after irradiation (λ > 400 nm) for 4 h in the presence of 9-EtG.

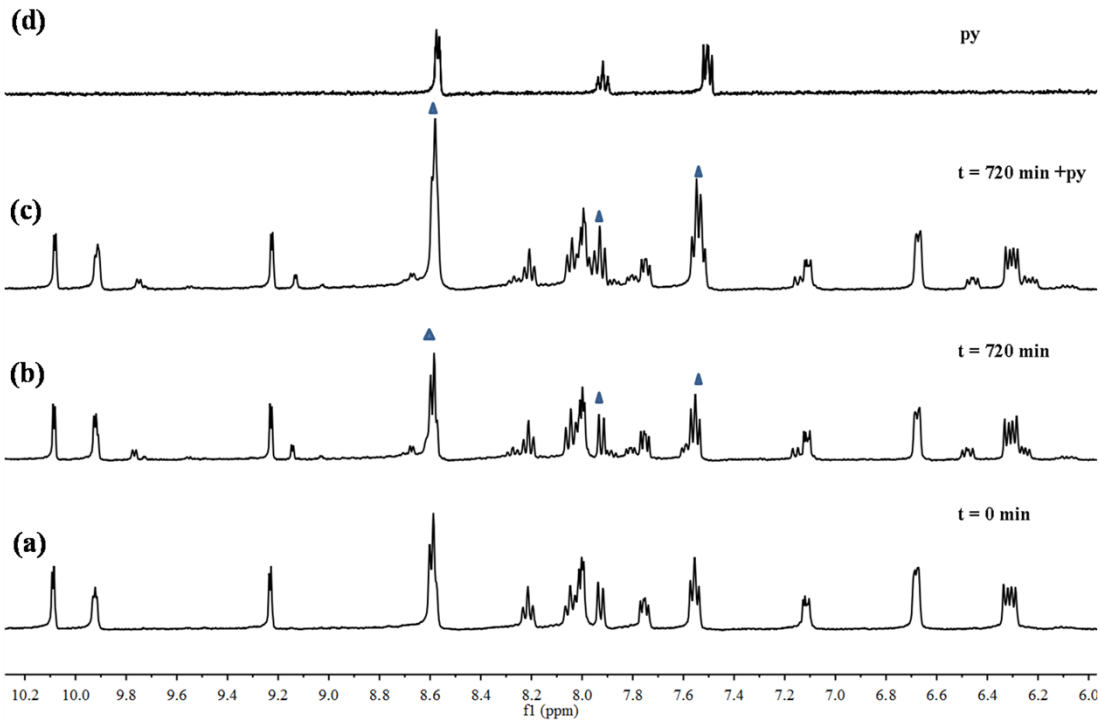

Figure S6. ^{1}H NMR spectra changes of **3** in CD_3COCD_3:D_2O (1:2) upon irradiation ($\lambda > 400$ nm). (a) before irradiation; (b) after irradiation for 12 h; (c) after irradiation for 12 h and addition of py; (d) ^{1}H NMR spectrum of py in CD_3COCD_3:D_2O (1:2). Chemical shifts of py are labeled by ▲.

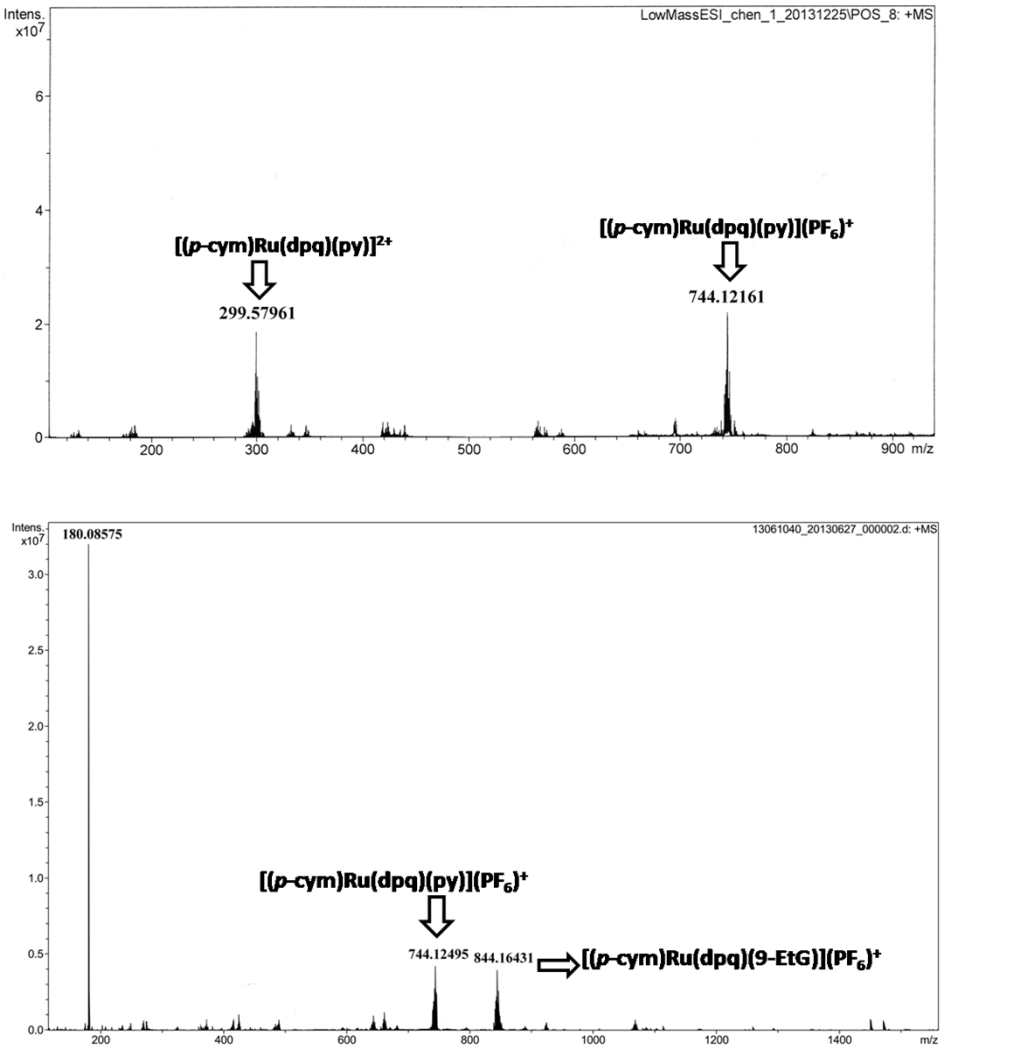

Figure S7. High-resolution ESI mass spectra of **2** in CH_3COCH_3:H_2O (1:2) (top) and after irradiation ($\lambda > 400$ nm) for 4 h in the presence of 9-EtG (bottom).

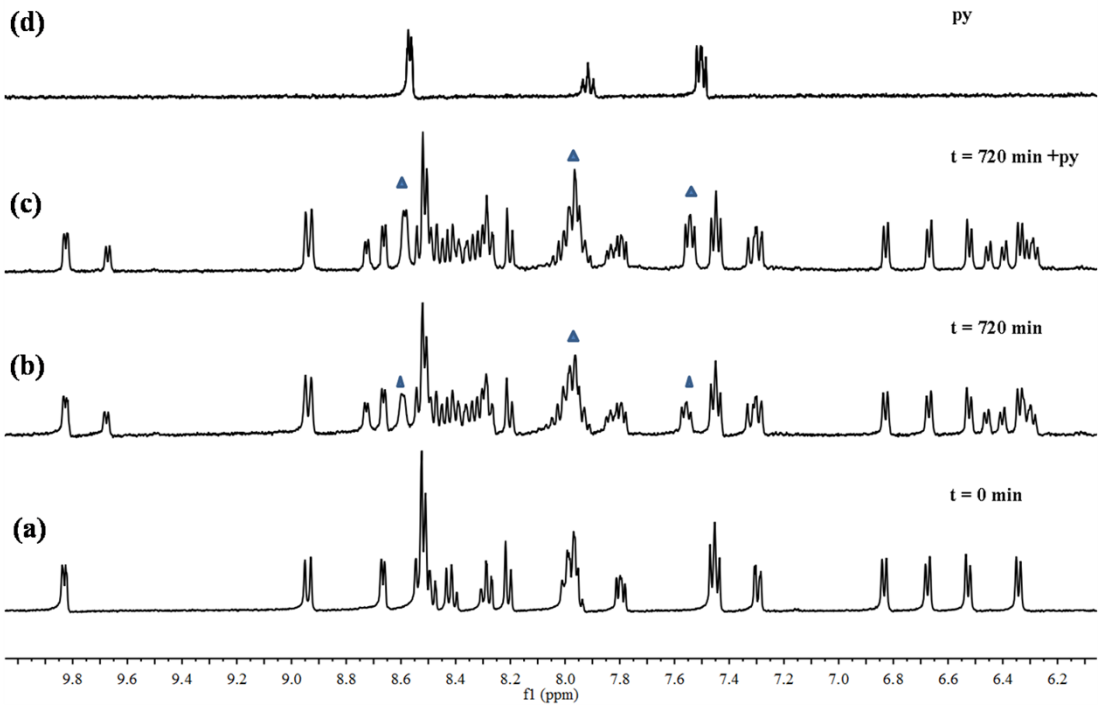

Figure S8. ^{1}H NMR spectra changes of **2** in CD_3COCD_3:D_2O (1:2) upon irradiation ($\lambda > 400$ nm). (a) before irradiation; (b) after irradiation for 12 h; (c) after irradiation for 12 h and addition of py; (d) ^{1}H NMR spectrum of py in CD_3COCD_3:D_2O (1:2). Chemical shifts of py are labeled by ▲.

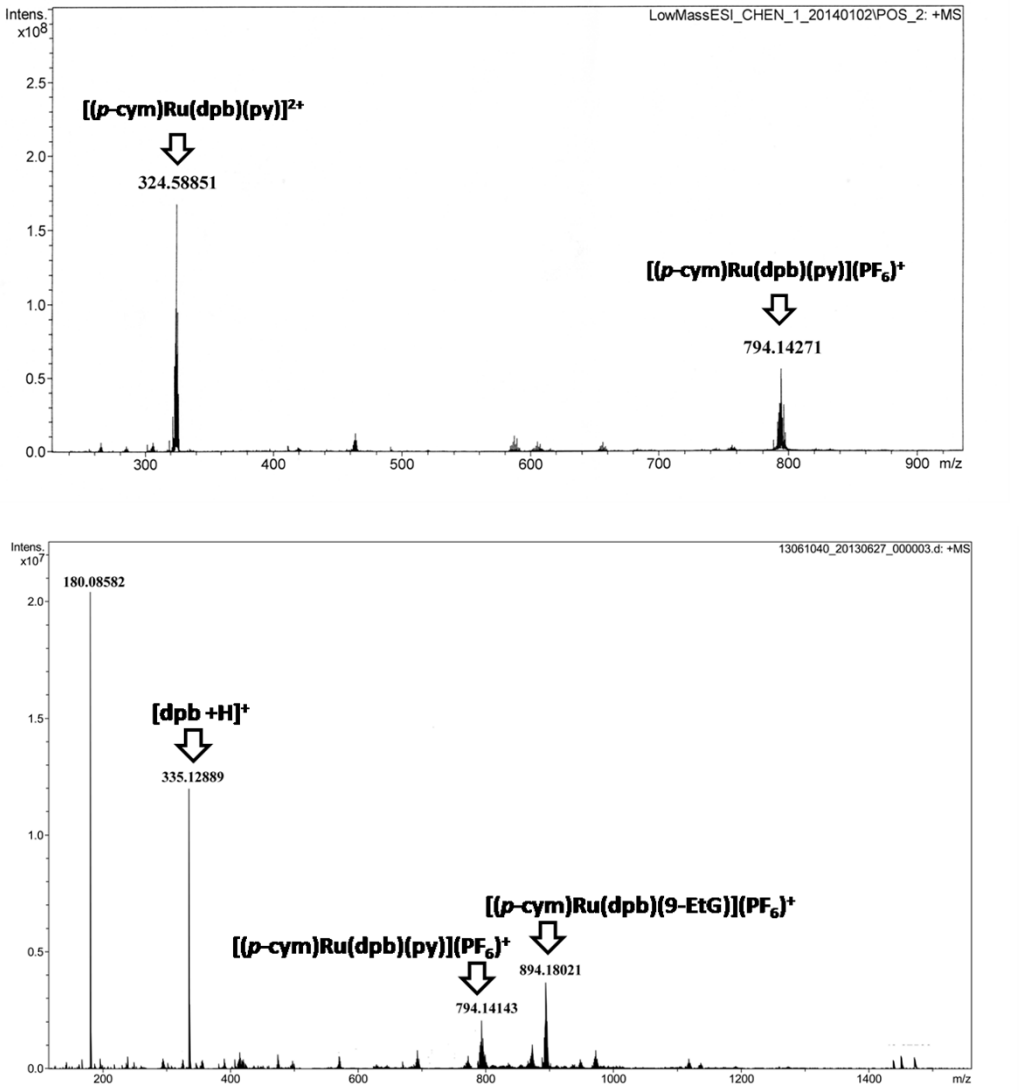

Figure S9. High-resolution ESI mass spectra of **1** in CH_3COCH_3:H_2O (1:2) (top) and after irradiation ($\lambda > 400$ nm) for 4 h in the presence of 9-EtG (bottom).

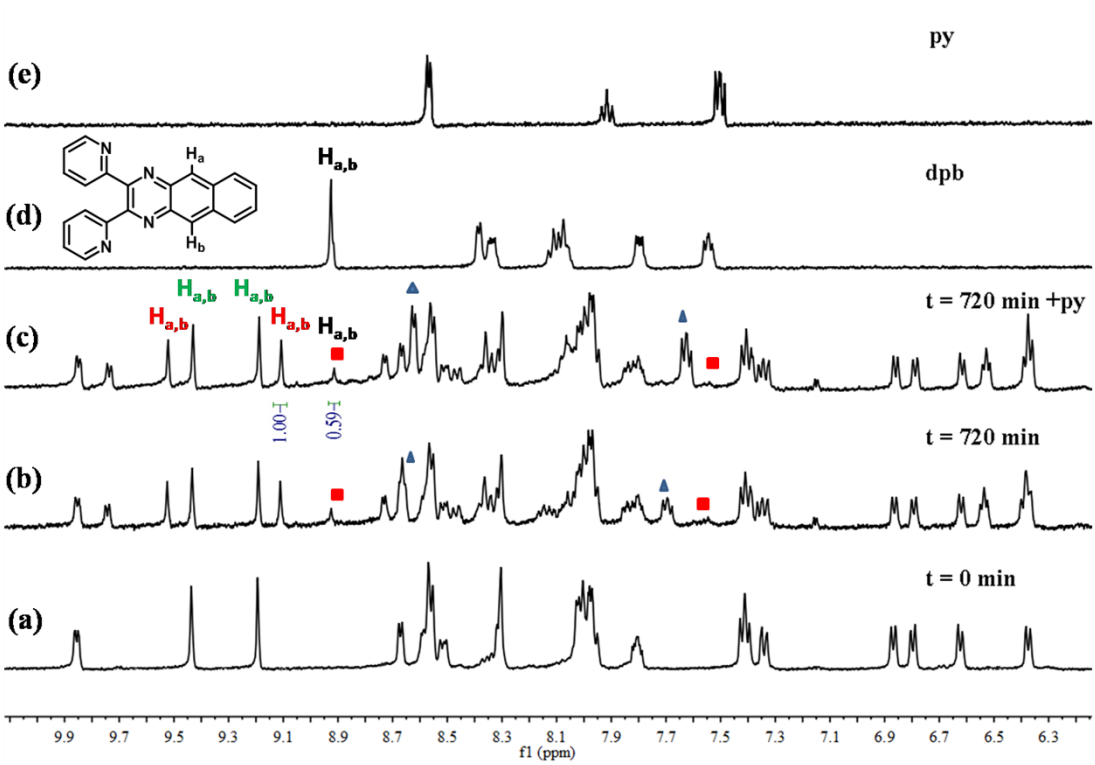

Figure S10. ^{1}H NMR spectra changes of **1** in CD_3COCD_3:D_2O (1:2) upon irradiation (λ > 400 nm). (a) before irradiation; (b) after irradiation for 12 h; (c) after irradiation for 12 h and addition of py; (d) ^{1}H NMR spectrum of dpb in CD_3COCD_3:D_2O (1:2); (e) ^{1}H NMR spectrum of py in CD_3COCD_3:D_2O (1:2) . Chemical shifts of py and dpb are labeled by ▲ and ■, respectively. $\mathbf{H_{a,b}}$, $\mathbf{H_{a,b}}$ and $\mathbf{H_{a,b}}$ indicate the chemical shifts of H_a and H_b of dpb in free dpb, **1**, and the py-leaving product.

Interestingly, the released py from **1** seems had some kind of interaction with **1**, leading to a remarkable downfield shift of its proton signals with respect to those of pure py in the same deuterated solvent.

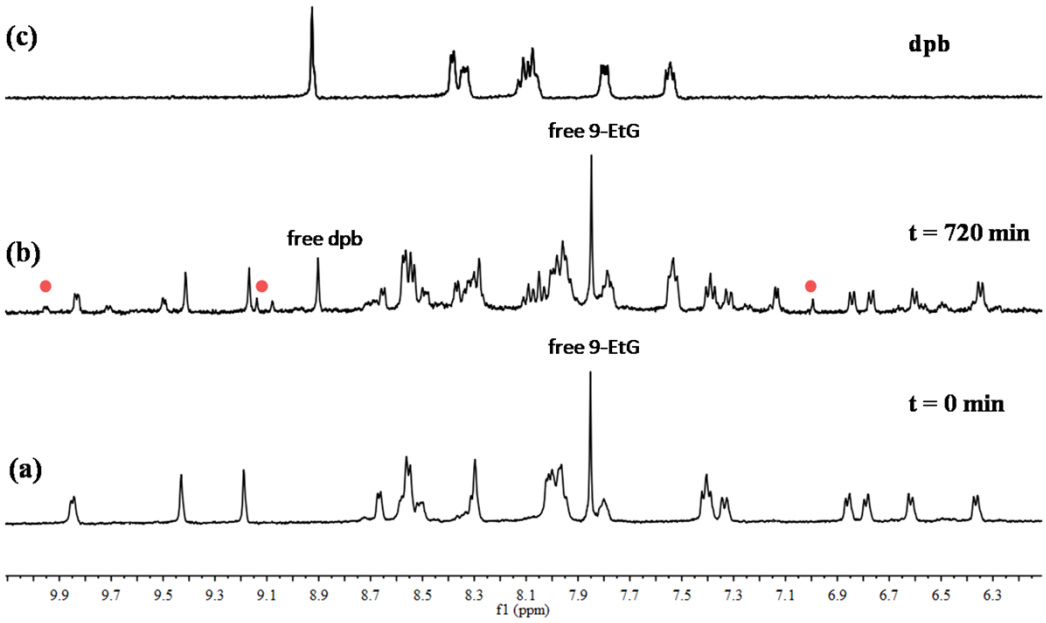

Figure S11. ^{1}H NMR spectra changes of **1** in CD_3COCD_3:D_2O (1:2) upon irradiation ($\lambda > 400$ nm) in the presence of excess 9-EtG. (a) before irradiation; (b) after irradiation for 12 h; (c) ^{1}H NMR spectrum of dpb in CD_3COCD_3:D_2O (1:2).

● indicates the resonant signals that were not observed in Figure S10(b) and (c), which may be attributed to the Ru(II) products bearing 9-EtG as ligand. For example, the singlet at 6.99 ppm may be ascribed to the aromatic proton, H(8), of the bond 9-EtG. Interestingly, the dpb-leaving product became predominant in this condition, as evidenced by the significantly enhanced intensity of the $H_{a,b}$ signal (singlet at 8.90 ppm) of the released dpb ligand. Additionally, the $H_{a,b}$ signals of the bond dpb ligand in the in-situ formed Ru(II) products are no longer double singlet, in line with the combination of both D_2O substituted and 9-EtG substituted products.

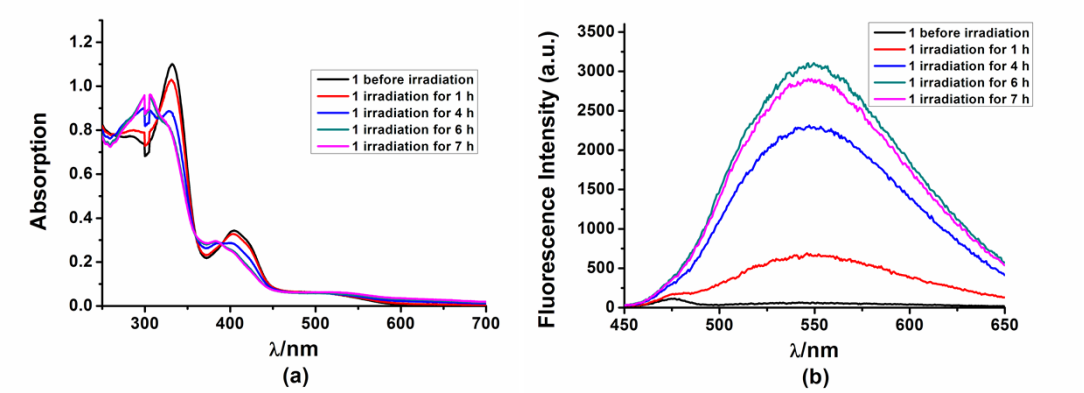

Figure S12. Absorption (a) and fluorescence emission (b) spectra changes of **1** (25 μM) in PBS (pH = 7.4) upon irradiation with λ > 550 nm.

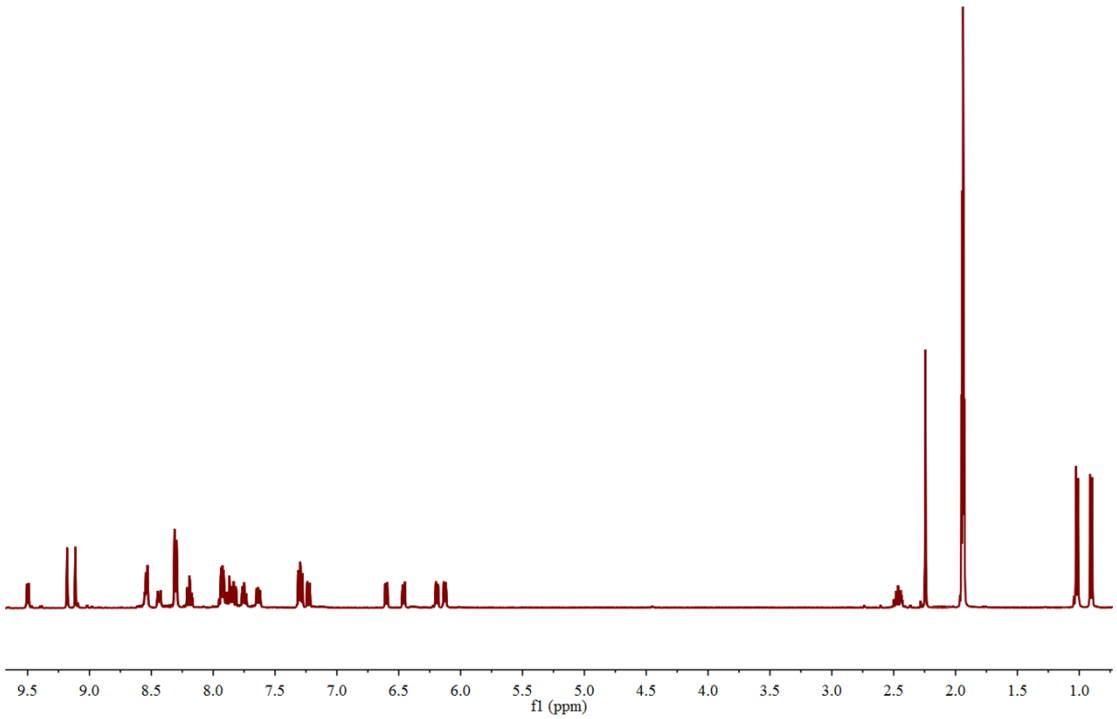

Figure S13. ^{1}H NMR spectrum of **1** in CD_3CN.

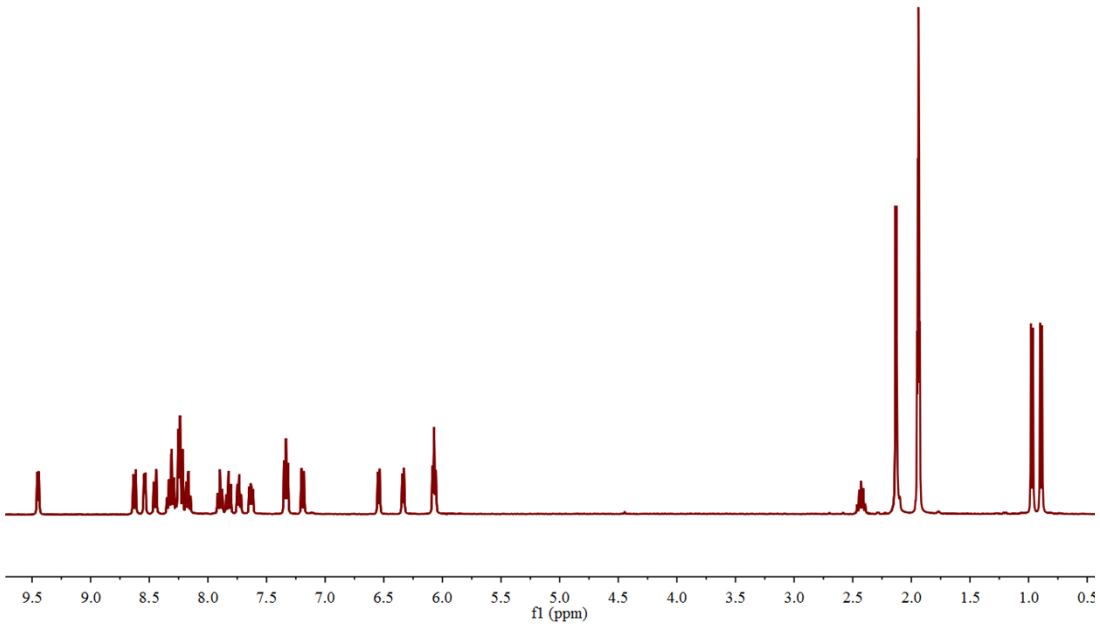

Figure S14. ^{1}H NMR spectrum of **2** in CD_3CN.

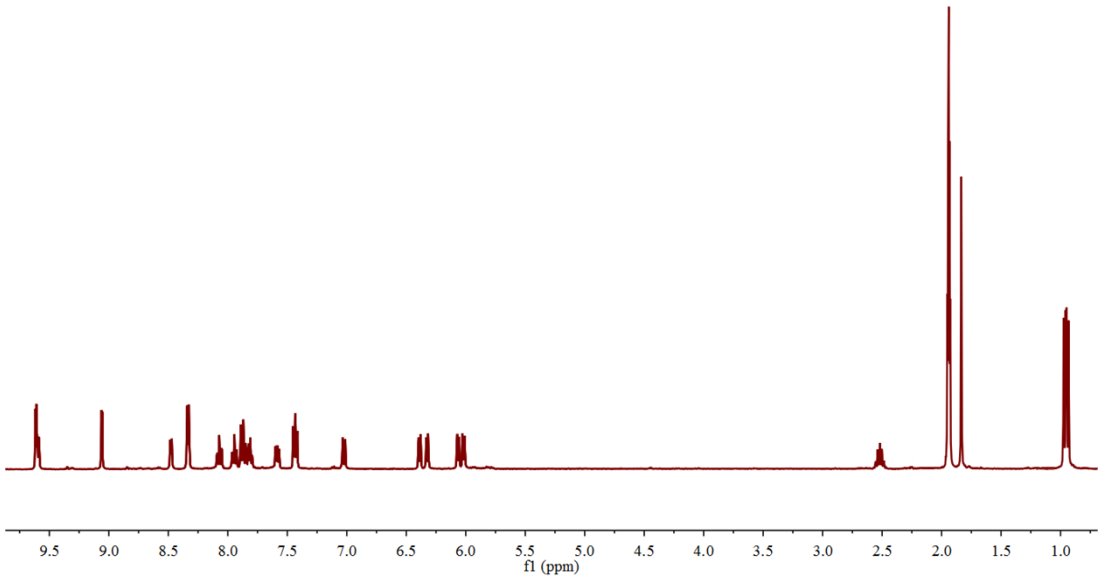

Figure S15. ^{1}H NMR spectrum of **3** in CD_3CN.

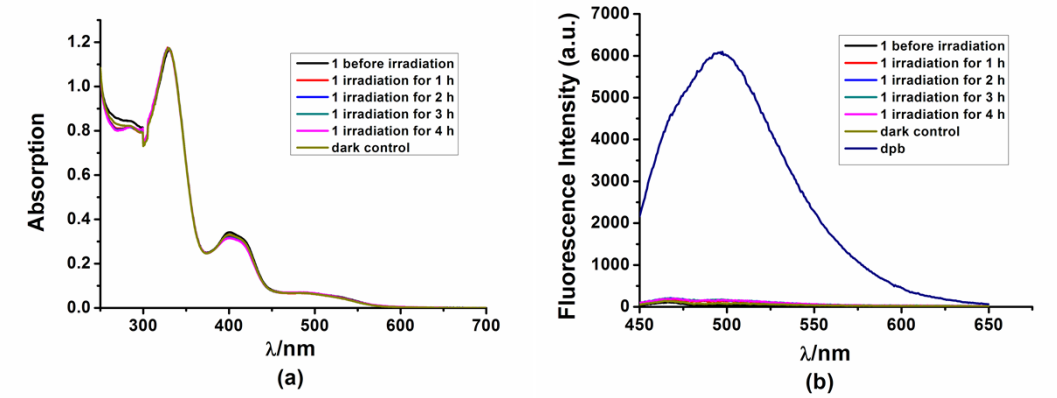

Figure S16. Absorption (a) and fluorescence emission (b) spectra changes of **1** (25 μM) in acetonitrile upon irradiation with λ > 400 nm.

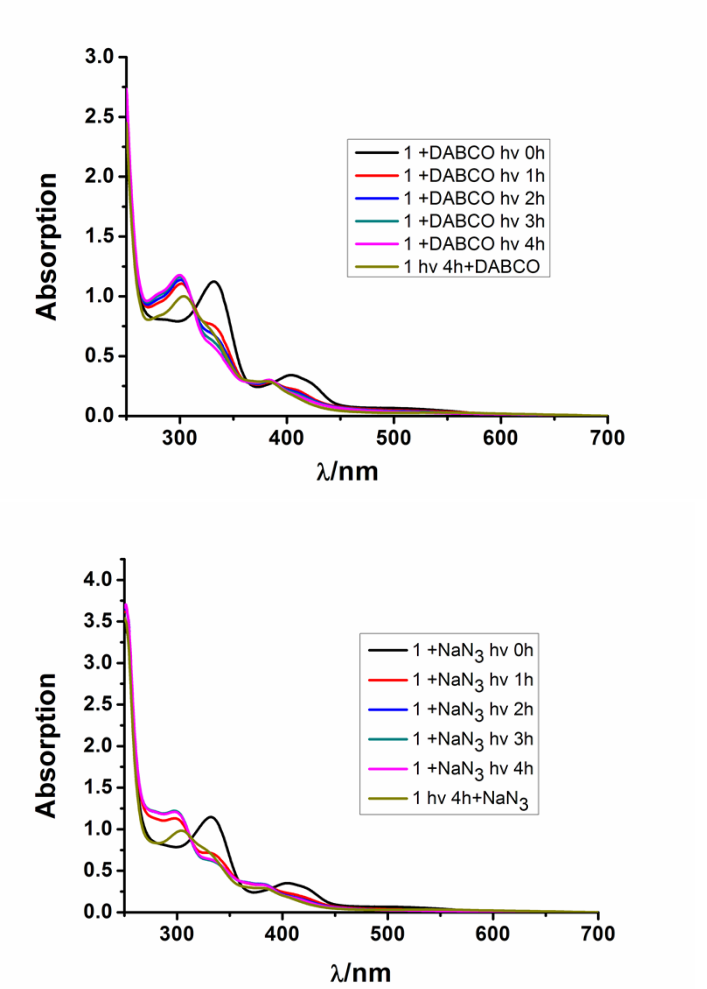

Figure S17. Absorption spectra changes of **1** (25 μM) in PBS buffer (pH = 7.4) upon irradiation at λ > 400 nm in the presence of 50 mM DABCO (top) or NaN_3 (bottom).

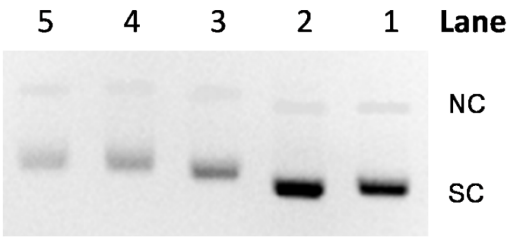

Figure S18. Agarose gel electrophoresis pattern of supercoiled pUC19 DNA (40 μg/mL) in air-saturated Tris-CH_3COOH/EDTA buffer (pH = 7.4) irradiated at λ > 550 nm for 90 min in the presence of varied concentrations of **1**. Lane 1: 100 μM of **1,** dark control; Lanes 2-5: 0, 25, 50, 100 μM of **1**.

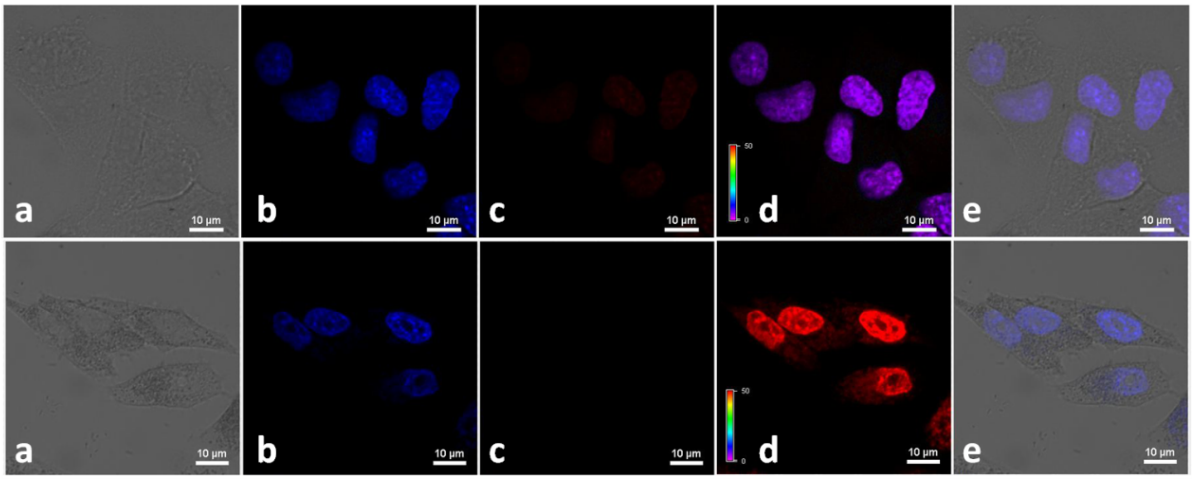

Figure S19. Confocal micrographs of the double-stained A549 cells by Hoechst 34580 and **1** with (top) or without (bottom) pre-illumination. a) bright field images; b) Hoechst 34580 fluorescence image upon excitation at 408 nm; c) fluorescence image of **1** upon excitation at 408 nm; d) the fluorescence intensity ratio of blue (b) to red (c); e) overlay of (a), (b) and (c).